Radiología 64 (2022) 445–455

RADIOLOGÍA

www.elsevier.es/rx

UPDATE IN RADIOLOGY

Dual-energy CT: Technical considerations and clinical applications

G.C. Fernández-Pérez[a,*], C. Fraga Piñeiro[b], M. Oñate Miranda[c], M. Díez Blanco[c], J. Mato Chaín[c], M.A. Collazos Martínez[c]

[a] *Servicio de Radiodiagnóstico, Hospital Universitario Río Hortega, Grupo Recoletas, Valladolid, Spain*
[b] *Técnico Aplicaciones Siemens Healthineers, General Electric Company, Spain*
[c] *Servicio de Radiodiagnóstico, Hospital Universitario Río Hortega, Valladolid, Spain*

Received 2 May 2022; accepted 20 June 2022

KEYWORDS
Dual energy;
Computed tomography;
Single-energy images;
Without virtual contrast;
Iodine map

Abstract Although dual-energy CT was initially described by Hounsfield in 1973, it remains underused in clinical practice. It is therefore important to emphasize the clinical benefits and limitations of this technique. Iodine mapping makes it possible to quantify the uptake of iodine, which is very important in characterizing tumors, lung perfusion, pulmonary nodules, and the tumor response to new treatments. Dual-energy CT also makes it possible to obtain virtual single-energy images and virtual images without iodinated contrast or without calcium, as well as to separate materials such as uric acid or fat and to elaborate hepatic iron overload maps. In this article, we review some of the clinical benefits and technical limitations to improve understanding of dual-energy CT and expand its use in clinical practice.

PALABRAS CLAVE
Energía dual;
Tomografía computarizada;
Imágenes monoenergéticas;
Sin contraste virtual;
Mapa de yodo

Energía Dual en TC. Consideraciones técnicas y aplicaciones clínicas

Resumen A pesar de que el concepto de doble energía en TC nace con Hounsfield en 1973, su uso clínico permanece infrautilizado, siendo importante incidir en los beneficios clínicos y limitaciones de esta técnica. La utilidad de imágenes de «mapa de yodo» permite valorar cuantitativamente la captación de yodo, de gran importancia en la caracterización de lesiones tumorales, en los mapas de perfusión pulmonar, en la naturaleza del nódulo pulmonar o en la respuesta tumoral a los nuevos tratamientos. Permite la obtención de imágenes

* Corresponding author.
E-mail address: gabriel.fdez.perez@gmail.com (G.C. Fernández-Pérez).

monoenergéticas virtuales, imágenes virtuales sin contraste yodado o sin calcio, separación de materiales como ácido úrico o de la grasa o mapas de sobrecarga férrica hepática. En esta revisión, revisamos algunos de los beneficios clínicos y limitaciones técnicas para mejorar su comprensión y ayudar a expandir su uso clínico.

Introduction

The concept of dual energy arose from the limitations of computed tomography (CT) in tissue discrimination, due to the fact that the density in Hounslow units (HU) depends on the linear attenuation coefficient *(μ)*, which has a considerable overlap between different structures. The linear attenuation coefficient is the sum of the photoelectric absorption effect that predominates in low-energy photons and the ''Compton'' scattering, which predominates in high-energy photons. While the Compton effect depends on the density of the material, the photoelectric effect has a directly proportional relationship to the atomic number of the tissue (Z^3).[1]

The idea of the use of dual energy is not new. In his 1973 article entitled ''*Computarized Transverse Axial Scanning*'', Godfrey Hounsfield observed that iodine and calcium could be differentiated using two acquisitions of the same slice with different kilovoltage.[1] It was in the 1980s that the first dual-energy CT appeared, designed to analyse osteoporosis studies. This CT performed two shots at different energy levels, but with about five seconds between one and the other, which meant a very high temporal coherence.[2] Nowadays there are scanners which use this method with much shorter acquisition intervals. In 2006, the first dual-source CT scanner was designed for wide clinical use, installing two tubes that acquired simultaneously at 80 kV and 140 kV. Later, scanners appeared that obtained dual energy with a single tube, obtaining two acquisitions with rapid switching; other systems obtain the spectral difference by means of two superimposed detector layers (one absorbs low energy and the other high energy) or also by dividing the X-ray beam with the use of two filters (gold and tin) in the X-ray tube, which absorb low and high energy photons respectively[3,4] (Fig. 1).

One of the most widespread clinical uses has classically been the analysis of kidney and ureter stone composition, as it can differentiate between calcium stones (for example calcium oxalate) and uric acids stones. It is also possible to differentiate periarticular calcifications with a uric acid composition (gout) from pyrophosphate crystals. In addition, it can provide two lots of images (with contrast and virtual non-contrast [VNC]) in a single acquisition performed after contrast administration, thanks to the decomposition and subtraction of the iodine from the original study. Calcium subtraction enables imaging of bone oedema in the bone.[5–7]

New perspectives are now opening up, however, such as the application of dual energy in oncology, not only to distinguish between a benign or malignant lesion, but also to observe post-treatment changes in almost the same way as continuous perfusion studies.[3] It is possible to obtain studies of perfusion at a particular point in time using iodine uptake maps, such as those obtained in the lung, called ''pulmonary perfused blood volume'' (PBV), which enable assessment of pulmonary perfusion defects in situations such as pulmonary embolism, in lung diseases such as COPD and even in situations of hypoxaemia in lung infections.[8] There are other utilities based on post-processing, generating single-energy images to highlight iodine uptake or reduce metal artifacts for example.

The aim of this article is, based on personal experience with dual-source units, to examine and highlight lesser-known and useful aspects of dual-energy studies which can be used routinely.

A quick recap on the principles of dual energy

We need to remember that the dual energy principle is based on the use of two X-ray energy spectra, which enable materials with high atomic number to be detected, visualised, quantified or subtracted. The algorithms used for tissue differentiation basically depend on two of their properties, their atomic number (Z) and their electronic density or mass (ρ). Dual energy is related to the ''linear attenuation coefficient'' (μ), expressed in the following formula[9]:

$$\mu = \frac{\mu}{\rho}(E, Z)\,\rho$$

where, $\frac{\mu}{\rho}$ is the mass attenuation coefficient, E is the energy used, Z is the atomic number and ρ the density. If you look closely, it is not only the atomic number that influences the attenuation, but also the energy of the photons and the density of the material (see below for single-energy images).

When the data is acquired with two different energies, such as 80 kV and 140 kV, tissues with high attenuation can be differentiated; for example, calcium (bone) and iodine, which in a conventional CT could overlap because they have similar Hounsfield units (HU). This is shown by calculating the ratio of the HU of the tissue or element acquired at low energy (80 kV) and high energy (140 kV). This concept is known as the CT number ratio.

$$CT\ number\ ratio = \frac{HU\,(80\,kV)}{HU\,(140\,kV)}$$

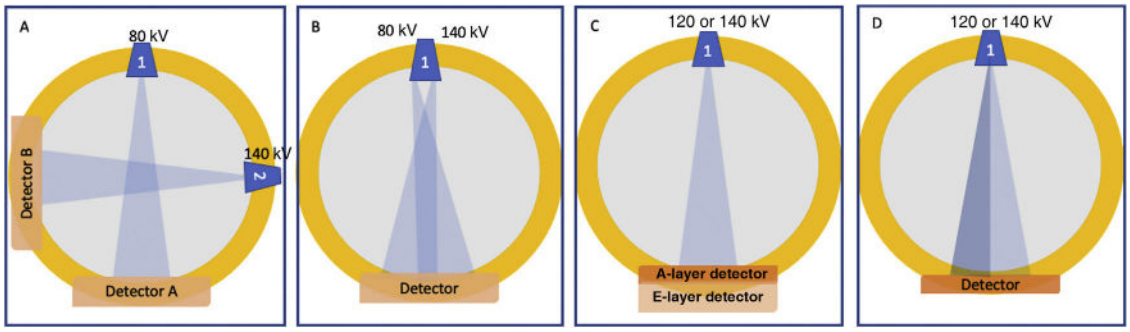

Figure 1 A) Dual source unit where one of the tubes emits high energy (140 kV) and a second low energy (80 kV), one perpendicular to the other. The high-energy tube has a tin (Sn) filter, which absorbs low-energy photons to lower noise and increase spectral differentiation efficiency. B) System where a single tube rotates rapidly, emitting exposures alternately to high (140 kV) and low energy (80 kV). C) System with a single tube that emits high energy (either 140 or 120 kV). Spectral separation occurs in the detector where an A layer of yttrium is positioned which separates low energy photons, allowing high energy photons to interact on a second B layer of gadolinium oxysulfide. D) Filter system in the X-ray tube which causes the beam to be divided into two low and high energy emissions (split-filter).

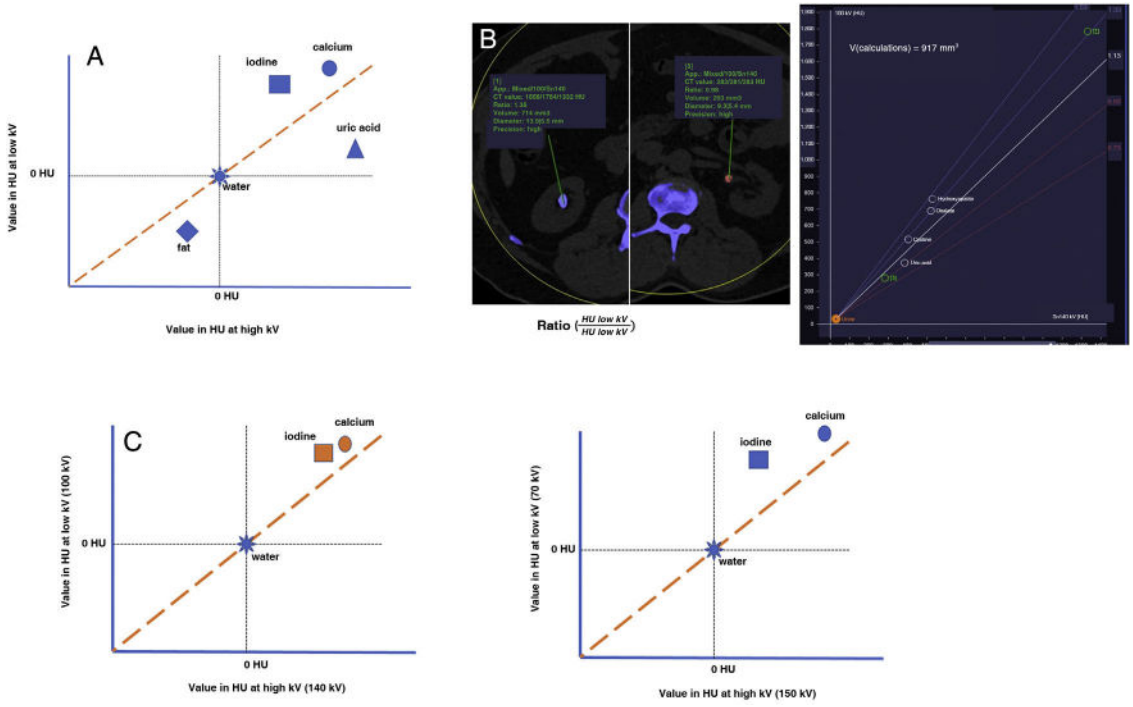

Figure 2 A) The differentiation of the materials depends on the absorption at high and low kV. The elements water and air are calibrated on CT at 0 and −1000 HU respectively. Elements with high atomic numbers, such as calcium and iodine, exhibit greater absorption at low energy; the low kV/high kV CT number ratio (called the dual-energy ratio) is greater than 1. In contrast, elements such as fat show greater absorption at high energies and so have higher HU values when high energy is applied. B) Blue calcium lithiasis. The ratio or density ratio is 1.35 (1784 HU/1332 HU) above the reference line. It is characteristic of both calcium and iodine (high Z elements) that they have higher absorption at low energy. Pink uric acid lithiasis. The ratio or density ratio is 0.98 (281 HU/283 HU), which is below the reference line. It has the characteristic (like fat) of having less absorption at low energies. C) The spectral separation is better when the differentiation or amplitude between the energies used is greater. A) Dual energy between 100 and 140 kV. B) Dual energy with 70 and 150 kV.

If we compare calcium and iodine, the values in HU are different at 80 kV (low energy) compared to high energy (140 kV), as they have different atomic numbers ($Z_{calcium} = 20$; $Z_{iodine} = 53$), which makes it possible to distinguish between the two elements (Fig. 2A and B).[10–12]

The differentiation of tissues is directly related to the greater spectrum of double energy used; thus, the greater the separation between the different kilovoltage used, the better the spectral separation (Fig. 2C). As we know, the linear attenuation coefficient depends on the photons (E = energy), such that the lower the kilovoltage of the first

energy, the lower the number of photons that reach the detector, causing greater noise in the image. This noise increase negatively affects the accuracy of the values in HU. To improve this limitation, some equipment incorporates a tin filter (Tin-Sn) with greater performance in the attenuation of low-energy photons.[10]

The differentiated materials are presented using their decomposition and each material can be calculated using an absorption algorithm. Thus, we can select images of iodine, forming ''iodine maps'', or if iodine is subtracted, images called ''VNC'' are created. The VNC have the advantage of reducing the radiation dose as they avoid performing acquisitions without contrast, especially in biphasic or triphasic protocols (kidney, liver, vascular, etc).[13]

The iodine map images are fused with the VNC images to enhance anatomical detail[12] (Fig. 3A). Similarly, other materials such as calcium are subtracted, eliminating the trabecular bone (virtual non-calcium images) and allowing other contents such as bone marrow oedema (bone marrow image) to be assessed (Fig. 3B).[7,14]

It should be remembered that dual energy has another benefit for clinical use, with the possibility of virtually forming monochromatic images with different energy (Fig. 4A). A conventional CT acquires with a polychromatic energy, meaning despite the fact that we carry out a study at, for example, 120 kV, the energy that reaches the detector is not uniform as it does so in a variable range of energy (polyenergetic). Dual energy can emulate images which would have been acquired with a single homogeneous source (for example 70 keV), hence called virtual monoenergetic (or monochromatic) images. These images can be generated at any energy, but due to limitations in quality and other technical considerations, the scanners obtain them from 40 to 200 keV.[15–18]

We need to remember that in low-energy images, materials with a higher atomic number (for example iodine) have higher contrast, a peculiarity due to the photoelectric effect with a direct relationship with the Z value. However, they have the drawback of increasing noise (fewer photons), as well as the ''beam hardening'' artefact. The use of specifically designed algorithms would improve this limitation (see below). At the other extreme, in high-energy virtual images, the Compton effect prevails, where contrast differentiation (iodine) is lost because image contrast depends on element density (ρ). However, they have the great advantage of eliminating beam hardening artefact and the clinical utility of reducing metal (prosthetic) artifacts.[15]

Dual energy quantification makes it possible not only to characterise lesions by measuring HU, but also with the amount of iodine in tissues (mg/dl). It can also calculate the effective atomic number (Z_{eff}) and the effective electron density (ρ_e) of a tissue with minimal errors.[16] A Z_{eff} map is a quantitative approach to differentiating materials by analysing changes in attenuation according to the energy. We know, through studies with phantoms, the Z_{eff} values of different materials. For example, the HU value of water is zero. However, the Z_{eff} value of water is 7.4. Mileto et al.[19] assessed the differentiation of renal cysts and renal lesions with enhancement by quantifying the Z_{eff} measurements, concluding that renal cysts without enhancement, including cysts with blood content (hyperdense), could be differentiated with a Z_{eff} cut-off value of 8.36, with a sensitivity of 91%.

Solutions to the most common limitations

Noise in low-energy monoenergetic images

We know the advantage of low-energy images in increasing contrast display (photoelectric effect), but they have the disadvantage of proportionally increasing image noise. Some CT units have improved on this problem with techniques called frequency-split (Monoenergetic Plus; Siemens Healthcare, Forchheim, Germany). They consist of using the low keV image and combining it with the one with lower noise and higher energy (close to 70 keV), thus improving the noise without losing contrast.[12,15]

Iodine map

To correctly evaluate iodine map images, an appropriate window range has to be selected. The selection has to be optimal to avoid either tissues such as fat or air having the appearance of enhancing or containing iodine. For this purpose, a good range is a width W 150 and a centre C 80. We have to bear in mind that perfusion maps (PBV) or bone marrow images sometimes require small adjustments in the window values to obtain appropriate diagnostic images.

It is important to remember that simple renal cysts, particularly if small in size, can appear coloured with the false impression of showing uptake, an artefact called ''pseudoenhancement''. This effect may be due to noise in the image, the acquisition technique itself or the energy (dose) used. One solution to correct this, as we have seen, is to analyse a Z_{eff} map or the monoenergetic images, assessing the morphology of the practically flat curve; that is, with similar HU in the high-energy and low-energy images (Fig. 5).[20,21]

Quantitative measurements made on the iodine map images (mg/dl of iodine) cannot be recalculated once these images have been sent to the picture archiving and communication system (PACS), as they are only obtained through specific post-processing, which is not supported by the Digital Imaging and Communications in Medicine (DICOM) system. Therefore, when the iodine map images are sent to the PACS, only a qualitative assessment can be performed based on the colour map.

Virtual non-contrast

VNC images are achieved by subtracting the iodine material. Sometimes, however, when the iodine concentration is very high, for example, in the aorta, the subtraction is not complete. This effect is due to the fact that, as we know, tissue attenuation depends on both atomic number and concentration. The use of high-energy (>120 keV) monoenergetic imaging can ameliorate this problem by removing the photoelectric effect.[22–24]

Sometimes there are elements with an atomic number very close to iodine (Z = 53), like barium (Z = 56), and it would also therefore be subtracted, so we would have complete

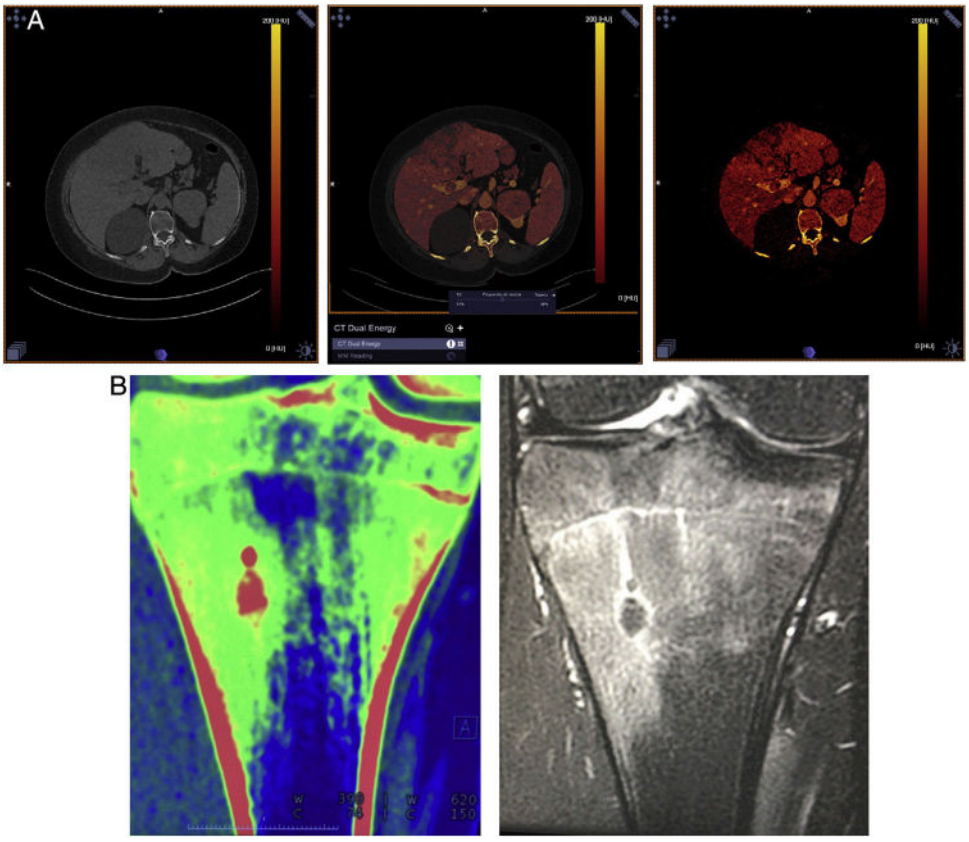

Figure 3 A) Single post-contrast acquisition. Axial plane image of the upper abdomen. Left-hand image, virtual non-contrast (VNC). Central image with iodine map merged with the anatomical image at 50%. Right-hand image, iodine map. B) 19-year-old male diagnosed with osteoid osteoma in the proximal tibial metaphysis. Dual-energy CT, coronal plane and ''bone oedema'' map image showing bone oedema adjacent to the nidus in green (red). MRI with coronal T2-weighted sequence, with fat saturation showing the extent of bone oedema similar to the CT study.

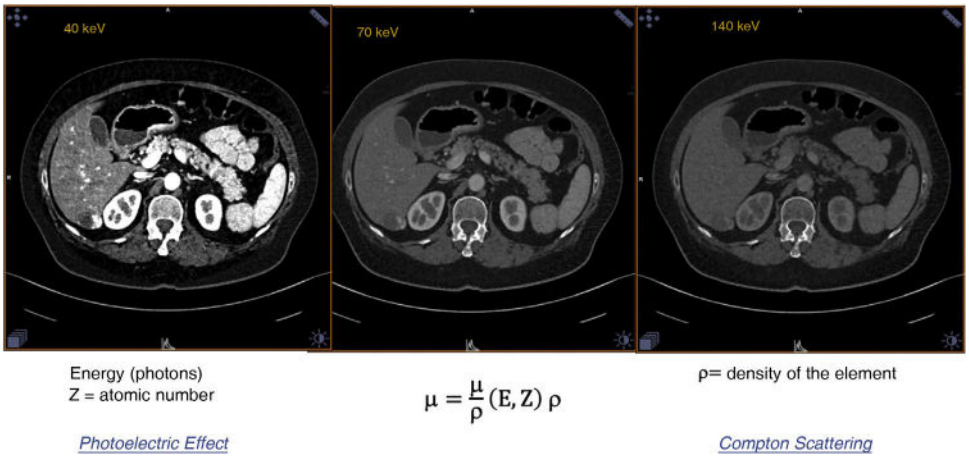

Figure 4 Single-energy images. In low energy images, the photoelectric effect predominates, showing greater contrast due to the influence of the atomic number (Z). However, in high-energy images, the Compton effect predominates, where the density depends on the density of the element in the tissues (ρ).

removal of both the intravenous and the oral contrast. Also, materials such as lipiodol for the visualisation of hepatocellular carcinoma become lost in the VNC images.

In the characterisation of adrenal lesions, there is a slight variation in HU between the measurements made with true non-contrast acquisition and those that would be obtained with the VNC technique. VNC overestimates the values by around ± 10 HU. The solution again is to visualise high-energy monoenergetic images, where the units are

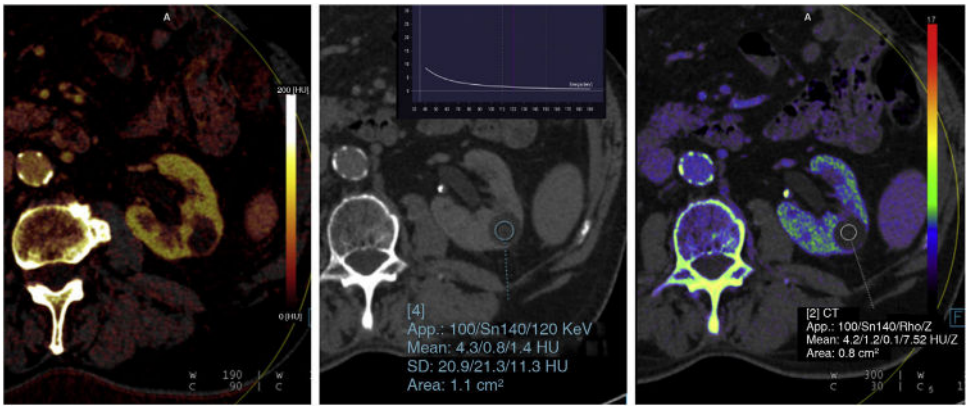

Figure 5 ''Pseudo-enhancement'' effect in cystic lesions. A) ''Iodine map'' image, showing a slightly heterogeneous left renal cyst that could suggest possible uptake. B) However, in the high energy single-energy image (120 keV) it has homogeneous hypodensity, with attenuation values of 1.4 HU and an attenuation curve of the different energies in the water range, correcting the pseudoenhancement phenomenon. C) Electron density map (Zeff/Rho), quantifying the lesion with Zeff and Rho values of 7.5 and 0.1 respectively (values characteristic of water).

practically similar to those obtained in a true non-contrast scan.[25]

Clinical applications

There are many clinical applications currently and there will be many more in the future. We discuss some of the most interesting and clinically established below.

Chest studies

One of the best known clinically is the use of dual energy in the diagnosis of pulmonary embolism (PE), not only for the visualisation of the thrombus, but also because it can show the perfusion alterations in the lung parenchyma by means of pulmonary perfusion maps called PBV. A greater number of perfusion defects correlates with the severity of the clinical picture and right heart overload, expressed as the increase in the ratio between the right ventricle and left ventricle diameters.[26–32] Also, the response to treatment can be assessed in patients in whom fibrinolysis is used, seeing the improvement within a few hours of starting treatment. A third advantage over conventional or single-energy CT is in subsegmental PE, as it demonstrates perfusion defects even when the occluded vessel is small and might go unnoticed. Re-evaluating the scans of patients where only perfusion defects were observed, the occluded vessel was found in 20% of the cases (Fig. 6).[26–28] The fourth scenario is being able to identify the perfusion defect, but that there is no occluded vessel despite re-analysing the study. There are several interpretations for this, the most plausible being that it cannot be demonstrated due to spatial resolution problems, probably because the vascular occlusion is microscopic. However, it could also be the case that these areas are not perfused by pulmonary arteries, but by systemic (bronchial) vessels, such that in a subsequent or arterial acquisition, this initial perfusion defect would have disappeared.[29] Similarly, pulmonary perfusion defects have been studied in patients with COPD or lung disorders, as recently seen in SARS-CoV-2 pneumonia.[32] In addition, the use of gases such as helium or xenon can assess ventilation abnormalities.

Other interesting utilities focus on the study of lung cancer, where iodine quantification can be used as a biomarker, being found in patients who express the VEGF gene and even differentiating adenocarcinomas with a low or high degree of differentiation.[33] Li et al[34] found significant differences in iodine concentrations between monoenergetic images at 40 and 100 keV in non-small cell lung cancer and between groups with negative and mild or moderately positive expression for the VEGF gene. Furthermore, these parameters also showed a significant and positive correlation with the expression level for VEGF ($r = 0.413$ and 0.393 respectively, $p < 0.05$). Chae et al[35] analysed the utility of double energy in the characterisation of malignancy of pulmonary nodules through contrast studies, reaching an accuracy of above 80% when the enhancement of the nodule was greater than 20 HU (Fig. 7).

Abdomen studies

Similar to the differentiation between calcium and uric acid in urolithiasis, liver fat or iron content can be determined using fat and iron overload quantification maps.[36]

Oncological studies have a special indication, taking advantage of iodine map and monoenergetic images. For example, using low-energy images (less than 50 keV) in pancreatic tumours (adenocarcinoma) increases the contrast and makes it possible to better assess the extension, invasion and staging of the cancer (Fig. 8).[37]

In hypervascular (neuroendocrine) tumours, iodine map images can quantify uptake changes as a tumour response to neoadjuvant (antiangiogenic) therapy. This tool would be used much like in any other hypervascular tumour, such as hepatocellular carcinoma, clear cell renal cell carcinoma or renal carcinoid tumours (Fig. 9). It is important for image acquisition to be at the appropriate phase, for example, to identify hepatocellular carcinoma with sufficient contrast delay to reach the late arterial phase. In kidney scans, it has been agreed to use the nephrographic

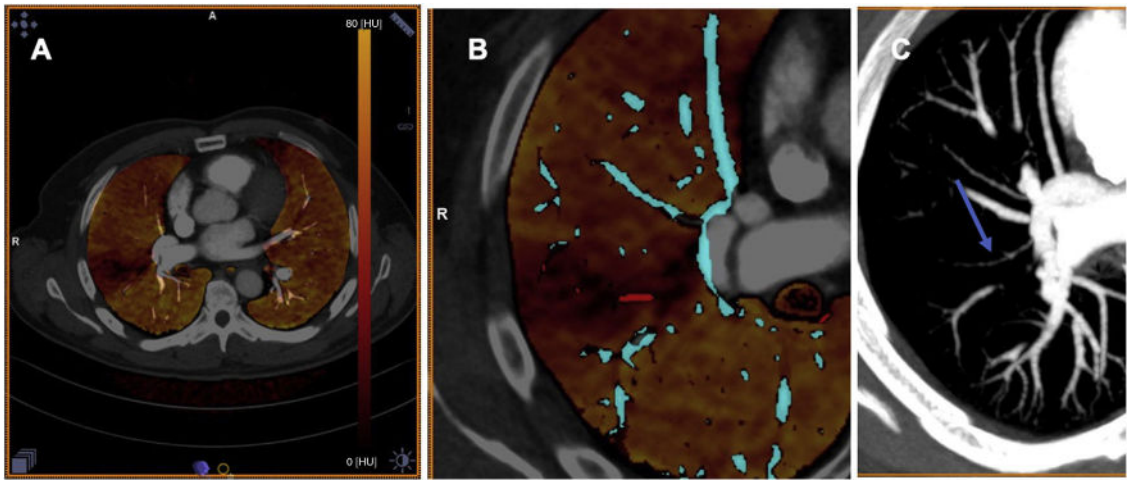

Figure 6 Follow-up scan in a 34-year-old female patient, six months after having a pulmonary embolism. A) Iodine map image showing a small peripheral triangular perfusion defect. B) The vascular analysis map shows a vessel with less contrast (red), which corresponds to a filiform vessel (C), as a consequence of a previous thromboembolism (lack of re-channelling).

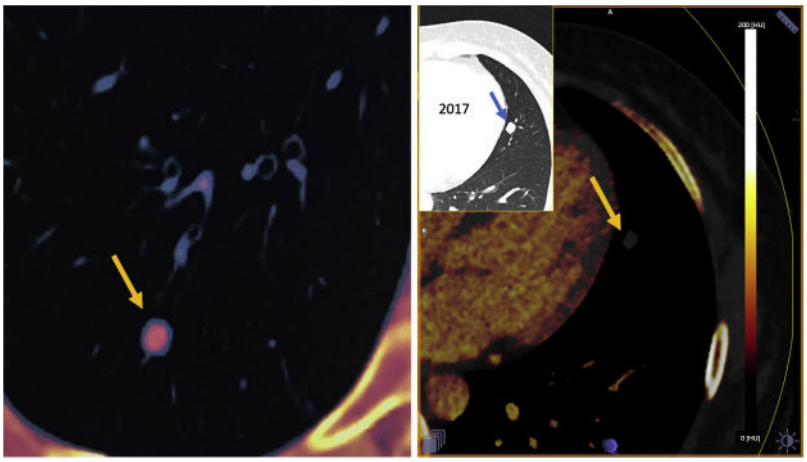

Figure 7 Pulmonary nodule study with dual-energy acquisition delayed for 3 min after administration of IV contrast (90 ml and flow rate of 3 ml/s). Dual energy analysis with ïodine mapänd colour scale for uptake greater than 20 HU (red). A) Patient with squamous cell head and neck tumour with a metastatic pulmonary nodule marked in red on the image due to uptake greater than 20 HU. B) Patient with stable nodule in follow-up without contrast uptake on the iodine map.

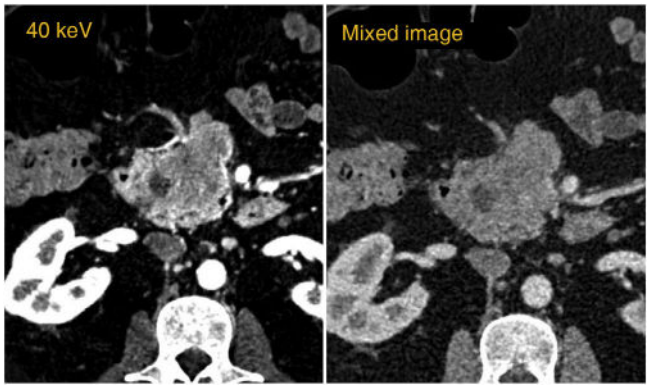

Figure 8 Patient with adenocarcinoma of the pancreas. Single-energy image at 40 keV showing higher contrast and better differentiation of tumour invasion than the mixed image (equivalent to 120 kV).

phase (90—110 s). In all these scans, acquisition without contrast is always avoided, as it is obtained automatically using the VNC images.[38,39]

In the diagnosis of patients with intestinal ischaemia, an increase in sensitivity is reported in studies with double energy compared to conventional CT, reaching values of 81% with the use of iodine maps and 100% with 40 keV monoenergetic images.[40]

In adrenal adenomas, a decrease in attenuation due to the presence of intracellular lipids was identified between 140 kV and 80 kV. Fifty percent of adenomas had a decrease in attenuation at 80 kV, while metastatic lesions had an increase in attenuation at 80 kV. With a decrease in attenuation at 80 kVp as an indicator of adenoma, dual-energy CT had a sensitivity of 50% with a specificity of 100% (PPV 100%).[41]

In patients with fatty liver disease, it is possible to analyse or quantify the liver fat fraction.[42,43] Patel et al[44]

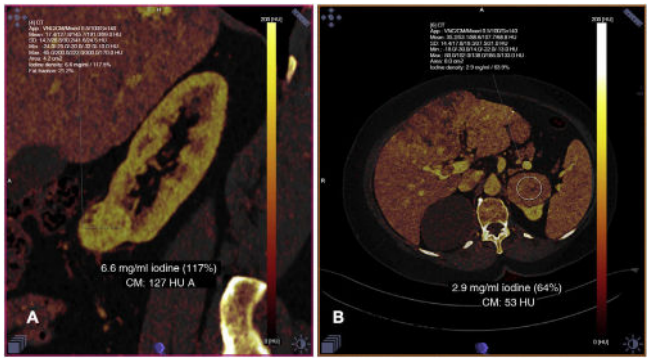

Figure 9 Iodine map in kidney tumours. A) Patient with tumour in the lower pole with high contrast uptake (6.6 mg/mL; equivalent to 117% with respect to the aorta), corresponding to a clear cell renal cell carcinoma. B) Patient with lesion in the upper pole of the left kidney with more moderate contrast uptake (2.9 mg/mL, which corresponds to 64% with respect to the aorta), with pathology result of oncocytoma. The iodine map also enables us to see a hepatic lesion (cholangiocarcinoma) and a tumour thrombus in the portal vein; the thrombus showing contrast uptake.

calculated the liver fat fraction (mg/mL) in virtual non-contrast images, obtaining a sensitivity of 90% and specificity of 61% with a threshold of 1027 mg/mL. Hyodo et al[45] reported values similar to MR spectroscopy, using a multimaterial decomposition algorithm (water, fat, iodine) in acquisitions with iodinated contrast. Similar results have been published more recently where they calculated the fat fraction in multiphasic contrast-enhanced studies with accuracy of more than 95%.[46–48]

Dual energy can also be used to calculate the liver iron fraction in haemochromatosis and haemosiderosis. The iron fraction can be obtained by calculating the variation in liver HU between the low and high kV data, between the data from the low and high energy virtual monochromatic images, and through three-material decomposition algorithms which enable iron to be differentiated from other materials (including fat), as well as quantifying the virtual iron content (VIC). It obtains sensitivity and specificity values similar to those obtained with the MRI T2* mapping technique.[36]

In the last ten years, several studies have investigated the role of contrast-enhanced CT in the diagnosis and evaluation of liver fibrosis. As a result, measurement of the extracellular volume fraction obtained from equilibrium liver CT has been proposed as a potential biomarker for liver fibrosis stratification. Bottari et al[49] found this value to be higher in patients with cirrhosis than in the control group, with significant differences ($p < 0.05$). This method has the intrinsic advantage of not requiring liver CT measurements without contrast, so it does not deviate from routine multiphase liver CT protocols.

Musculoskeletal studies

Monosodium urate crystal deposits (gout) can be identified in joints and tendons and differentiated from joint disease caused by calcium pyrophosphate crystal deposition. In the same way we quantify liver iron, we can find iron deposits in the synovium for the diagnosis of pigmented villonodular synovitis.[50]

Another advantage is identifying bone marrow oedema by differentiation and subtraction of fatty marrow and bone, along with obtaining ''virtual non-calcium'' images (similar to iodine subtraction in ''virtual non-contrast'' imaging). It can therefore show oedema in fractures, making it useful in vertebral fractures to identify whether or not they are acute, or in any other fracture where the solution of continuity in the cortical bone is subtle in the morphological images, as occurs in stress or insufficiency fractures.[14]

In investigations of myeloma, dual-energy CT can potentially assess typical myeloma lesions and may even be able to find active myeloma lesions.[51,52] It may also be helpful in patients with bone metastases, where the use of monoenergetic images (low energy 40 or 50 keV) differentiates the metastases better by increasing tissue contrast.[53]

Cardiovascular studies

Cardiac stress studies (adenosine) performed with dual energy increase the sensitivity for coronary lesions with haemodynamically significant stenosis when assessing myocardial perfusion defects in the affected vascular territory, reaching a sensitivity of 77% and specificity of 94%, correlating with cardiac MRI ($r = 0.6$; $p < 0.05$).[54]

Acquisitions made at three minutes can determine late contrast uptake to differentiate between scarring related to old infarction and scar fibrosis due to other causes, and may even enable quantification of the extracellular volume of the myocardium as in T1-mapping studies carried out in MRI.[54–57]

In vascular studies the amount of contrast can be reduced, an important factor in patients with renal impairment, obtaining low-energy monoenergetic images. Non-contrast acquisition can be eliminated in scans of the aorta (and vascular scans in general), as the VNC image is obtained automatically, with this being particularly important in acute aortic syndromes or in vascular stent leaks.[58]

Silicone breast implants

Dual-energy CT may be a simple and readily available technique for evaluating rupture of silicone breast implants. The photoelectric effect of silicon ($Z = 14$) is used, showing high contrast in low kilovoltage monoenergetic images. Silicone maps can be made, assessing intra- and extracapsular rupture zones, as well as the association with the infiltration of the substance into the lymph nodes[59,60] (Fig. 10).

Conclusions

To sum up, dual-energy CT scanning enables differentiation of elements with high HU values such as calcium or iodine, which would overlap on a conventional CT. By subtracting the known element, we can obtain iodine maps, VNC, virtual non-calcium or bone marrow oedema images. The amount of iodine that enhances a lesion can be quantified and elements can be quantitatively differentiated by

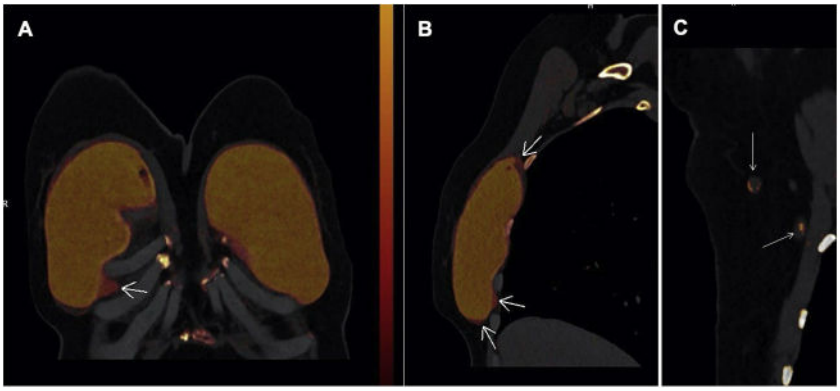

Figure 10 Rupture of right breast prosthesis. Dual energy CT scan without IV contrast (silicon map) as a consequence of photoelectric effect on silica material (Z = 14). A) Coronal plane showing silicon material outside the prosthesis (extracapsular rupture). B) Sagittal plane showing the rupture zones (arrows), both superior and inferior. C) Lymph node involvement due to accumulation of silicon related to the rupture (arrows).

their Z_{eff} value. Other elements can also be differentiated, such as fat in fatty liver disease and adrenal adenomas. Dual-energy CT also enables the amount of iron to be quantified in patients with liver iron overload in a similar way to MRI. The photoelectric effect of certain substances such as silicone can be used to search for ruptured breast implants.

The dual energy technique is based on the difference in HU obtained for each material in the high and low energy data, with the option of obtaining virtual images at different monochromatic energies. These images make use of the photoelectric effect to differentiate materials with high atomic number by showing higher image contrast, or the Compton scatter effect to reduce beam hardening artifacts and metal artifacts.

Funding

This work was not subsidised and nor was any financial aid received from any public or private institution.

Authorship

1 Responsible for study integrity: GCFP, CFP, MOM, JMC and MDB.
2 Study conception: GCFP, MDB, CFP and MACM.
3 Study design: GCFP, MDB, MOM and MACM.
4 Data collection: MOM, CFP, MACM and JMC.
5 Data analysis and interpretation: GCFP, CFP, MDB and MOM.
6 Statistical processing: GCFP, MDB and MOM.
7 Literature search: GCFP, JMC, MOM, MDB and MACM.
8 Drafting of the article: GCFP, MDB, MOM, CFP and JMC.
9 Critical review of the manuscript with intellectually relevant contributions: MOM, MDB, CPF and MACM.
10 Approval of the final version: GCFP, MDB, CFP, MOM, JMC and MACM.

Conflicts of interest

We declare that there are no conflicts of interest as this work was not subsidised and nor was any financial aid received from any public or private institution.

References

1. Hounsfield GN. Computerized transverse axial scanning (tomography): Part I. Description of system. 1973. Br J Radiol. 1995;815:H166–72.
2. Raymakers JA, Hoekstra O, van Putten J, Kerkhoff H, Duursma SA. Fracture prevalence and bone mineral mass in osteoporosis measured with computed tomography and dual energy photon absorptiometry. Skeletal Radiol. 1986;15:191–7.
3. Goo HW, Goo JM. Dual-energy CT: new horizon in medical imaging. Korean J Radiol. 2017;4:555–69.
4. Megibow AJ, Kambadakone A, Ananthakrishnan L. Dual-energy computed tomography: image acquisition, processing, and workflow. Radiol Clin North Am. 2018;4:507–20.
5. McGrath TA, Frank RA, Schieda N, Blew B, Salameh JP, Bossuyt PM, et al. Diagnostic accuracy of dual-energy computed tomography (DECT) to differentiate uric acid from non-uric acid calculi: systematic review and meta-analysis. Eur Radiol. 2020;30:2791–801.
6. Murray N, Darras KE, Walstra FE, Mohammed MF, McLaughlin PD, Nicolaou S. Dual-energy CT in evaluation of the acute abdomen. Radiographics. 2019;1:264–86.
7. Wong WD, Shah S, Murray N, Walstra F, Khosa F, Nicolaou S. Advanced musculoskeletal applications of dual-energy computed tomography. Radiol Clin North Am. 2018;4:587–600.
8. Fuld MK, Halaweish AF, Haynes SE, Divekar AA, Guo J, Hoffman EA. Pulmonary perfused blood volumen with dual-energy CT as surrogate for pulmonary perfusion assessed with dynamic multidetector CT. Radiology. 2013;267:747–56.
9. McCollough CH, Boedeker K, Cody D, Duan X, Flohr T, Halliburton SS, et al. Principles and applications of multi-energy CT: report of AAPM Task Group 291. Med Phys. 2020;47:e881–912, http://dx.doi.org/10.1002/mp.14157.
10. Wortman JR, Sodickson AD. Pearls, pitfalls, and problems in dual-energy computed tomography imaging of the body. Radiol Clin North Am. 2018;4:625–40.
11. Michalak G, Grimes J, Fletcher J, Halaweish A, Yu L, Leng S, et al. Technical note: Improved CT number stability across

patient size using dual energy CT virtual monoenergetic imaging. Med Phys. 2016;1:513–7.
12. McCollough CH, Leng S, Yu L, Fletcher JG. Dual- and multi-energy CT: Principles, technical approaches, and clinical applications. Radiology. 2015;3:637–53.
13. Parakh A, Macri F, Sahani D. Dual energy computed tomography: dose reduction, series reduction, and contrast load reduction in dual-energy computed tomography. Radiol Clin North Am. 2018;56:601–24.
14. Kaup M, Wichmann JL, Scholtz JE, Beeres M, Kromen W, Albrecht MH, et al. Dual-energy CT based display of bone marrow edema in osteoporotic vertebral compression fractures: impact on diagnostic accuracy of radiologists with varying levels of experience in correlation to MR Iiaging. Radiology. 2016;280:510–9.
15. Patel BN, Marin D. Strategies to improve image quality on dual-energy computed tomography. Radiol Clin North Am. 2018;56:641–7.
16. Yu L, Christner JA, Wang J, Fletcher JG, McCollough CH. Virtual monochromatic imaging in dual-energy CT: radiation dose and imaging quality. Med Phys. 2011;38:12.
17. D'Angelo T, Cicero G, Mazziotti S, Ascenti G, Albrecht M, Martin SS, et al. Dual energy computed tomography virtual monoenergetic imaging: technique and clinical solutions. Br J Radiol. 2019;92:20180546.
18. Albrecht MH, Vogl TJ, Martin SS, Nance JW, Duguay TM, Wichmann JL, et al. Review of clinical applications for virtual monoenergetic dual-energy CT. Radiology. 2019;293:260–71.
19. Mileto A, Allen BC, Pietryga JA, Farjat AE, Zarzour JG, Bellini D, et al. Characterization of incidental renal mases with dual-energy CT: diagnostic accuracy effective atomic number maps for discriminating noenhancing cyst from enhancing masses. AJR Am J Roentgenol. 2017;209:W221–30, http://dx.doi.org/10.2214/AJR.16.17325.
20. Li G, Dong J, Huang W, Zhang Z, Wang D, Zou M, et al. Establishment of a novel system for the preoperative prediction of adherent perinephritic fat (APF) occurrence based on a multimode and multiparameter analysis of dual-energy CT. Transl Androl Urol. 2019;8:421–31.
21. Laukamp KR, Zopfs D, Wagner A, Lennartz S, Pennig L, Borggrefe J, et al. CT artifacts from port systems: virtual monoenergetic reconstructions from spectral-detector CT reduce artifacts and improve depiction of surrounding tissue. Eur J Radiol. 2019;121:108733, http://dx.doi.org/10.1016/j.ejrad.2019.108733.
22. Wortman JR. Dual-energy computed tomography: technology and challenges. Radiol Clin North Am. 2018;56:497–506.
23. Bae JS, Lee DH, Joo I, Jeon SK, Han JK. Utilization of virtual non-contrast images derived from dual-energy CT in evaluation of biliary stone disease: virtual non-contrast image can replace true non-contrast image regarding biliary stone detection. Eur J Radiol. 2019;116:34–40.
24. Patel AA, Sutphin PD, Xi Y, Abbara S, Kalva SP. Arterial Phase CTA replacement by a virtual arterial phase reconstruction from a venous phase CTA: preliminary results using detector-based spectral CT. Cardiovasc Intervent Radiol. 2019;42:250–9.
25. Connolly MJ, McInnes MDF, El-Khodary M, McGrath TA, Schieda N. Diagnostic accuracy of virtual non-contrast enhanced dual-energy CT for diagnosis of adrenal adenoma: a systematic review and meta-analysis. Eur Radiol. 2017;27:4324–35.
26. Lu GM, Wu SY, Yeh BM, Zhang LJ. Dual-energy computed tomography in pulmonary embolism. Br J Radiol. 2010;83:707–18.
27. Singh R, Nie RZ, Homayounieh F, Schmidt B, Flohr T, Kalra MK. Quantitative lobar pulmonary perfusion assessment on dual-energy CT pulmonary angiography: applications in pulmonary embolism. Eur Radiol. 2020;30:2535–42, http://dx.doi.org/10.1007/s00330-019-06607-9.
28. Okada M, Kunihiro Y, Nakashima Y, Nomura T, Kudomi S, Yonezawa T, et al. Added value of lung perfused blood volume images using dual-energy CT for assessment of acute pulmonary embolism. Eur J Radiol. 2015;84:172–7.
29. Pontana F, Faivre JB, Remy-Jardin M, Flohr T, Schmidt B, Tacelli N, et al. Lung perfusion with dual-energy multidetector-row CT (MDCT): feasibility for the evaluation of acute pulmonary embolism in 117 consecutive patients. Acad Radiol. 2008;15:1494–504.
30. Weidman EK, Plodowski AJ, Halpenny DF, Hayes SA, Perez-Johnston R, Zheng J, et al. Dual- energy CT angiography for detection of pulmonary emboli: Incremental benefit of iodine maps. Radiology. 2008;289:546–53.
31. Rajiah P, Tanabe Y, Partovi S, Moore A. State of the art: utility of multi-energy CT in the evaluation of pulmonary vasculature. Int J Cardiovasc Imaging. 2019;35:1509–24.
32. Fernández-Pérez GC, Oñate Miranda M, Fernández-Rodríguez P, Velasco-Casares M, Corral de la Calle MA, Franco López A, et al. SARS-CoV-2: cómo es, cómo actúa y cómo se expresa en la imagen. Radiologia. 2021;63:115–26, http://dx.doi.org/10.1016/j.rx.2020.10.006.
33. Odisio EG, Truong MT, Duran C, de Groot PM, Godoy MC. Role of dual-energy computed tomography in thoracic oncology. Radiol Clin North Am. 2018;56:535–48.
34. Li GJ, Gao J, Wang GL, Zhang CQ, Shi H, Deng K. Correlation between vascular endothelial growth factor and quantitative dual-energy spectral CT in non-smallcell lung cancer. Clin Radiol. 2016;71:363–8.
35. Chae EJ, Song JW, Seo JB, Krauss B, Jang YM, Song KS. Clinical utility of dual-energy CT in the evaluation of solitary pulmonary nodules: initial experience. Radiology. 2008;249:671–81.
36. Werner S, Krauss B, Haberland U, Bongers M, Starke U, Bakchoul T, et al. Dual-energy CT for liver iron quantification in patients with haematological disorders. Eur Radiol. 2019;29:2868–77.
37. El Kayal N, Lennartz S, Ekdawi S, Holz J, Slebocki K, Haneder S, et al. Value of spectral detector computed tomography for assessment of pancreatic lesions. Eur J Radiol. 2019;118:215–22.
38. Bellini D, Panvini N, Laghi A, Marin D, Patel BN, Wang CL, et al. Systematic review and meta-analysis Investigating the diagnostic yield of dual-energy CT for renal mass assessment. AJR Am J Roentgenol. 2019;5:1–10, http://dx.doi.org/10.2214/ajr.18.20625.
39. Morgan DE. The role of dual-energy computed tomography in assessment of abdominal oncology and beyond. Radiol Clin North Am. 2018;56:565–85.
40. Lourenco PDM, Rawski R, Mohammed MF, Khosa F, Nicolaou S, McLaughlin P. Dual-energy CT iodine mapping and 40-keV monoenergetic applications in the diagnosis of acute bowel ischemia. AJR Am J Roentgenol. 2018;211:564–70, http://dx.doi.org/10.2214/ajr.18.19554.
41. Gupta RT, Ho LM, Marin D, Boll DT, Barnhart HX, Nelson RC. Dual-energy CT for characterization of adrenal nodules: initial experience. AJR Am J Roentgenol. 2010;194:1479–83, http://dx.doi.org/10.2214/ajr.09.3476.
42. Artz NS, Hines CD, Brunner ST, Agni RM, Kühn JP, Roldan-Azate A, et al. Quantification of hepatic steatosis with dual-energy computed tomography: comparison with tissue reference standards and quantitative magnetic resonance imaging in the ob/ob mouse. Invest Radiol. 2012;47:603–10.
43. Kramer H, Pickhardt PJ, Kliewer MA, Hernandeo D, Chen GH, Zagzebski JA, et al. Accuracy of liver fat quantification with advanced CT, MRI, and ultrasound techniques: prospective comparison with MR spectroscopy. Am J Roentgenol. 2017;208:92–100, http://dx.doi.org/10.2214/AJR.16.16565.
44. Patel BN, Kumbla RA, Berland LL, Fineberg NS, Morgan DE. Material density hepatic steatosis quantification

on intravenous contrast-enhanced rapid kilovolt (peak) switching single-source dual-energy computed tomography. J Comput Assisted Tomography. 2013;37:904–10, http://dx.doi.org/10.1097/rct.0000000000000027.
45. Hyodo T, Yada N, Hori M, Maenishi O, Lamb P, Sasoki K, et al. Multimaterial decomposition algorithm for the quantification of liver fat content by using fast-kilovolt-peak switching dual-energy CT: clinical evaluation. Radiology. 2017;283:108–18, http://dx.doi.org/10.1148/radiol.2017160130.
46. Hur BY, Lee JM, Hyunsik W, Lee KB, Joo L, Han JK, et al. Quantification of the fat fraction in the liver using dual-energy computed tomography and multimaterial decomposition. J Comp Assis Tomogr. 2014;38:845–52, http://dx.doi.org/10.1097/rct.0000000000000142.
47. Guo Z, Blake GM, Li K, Liang W, Zhang W, Zhang Y, et al. Liver fat content measurement with quantitative CT validated against MRI proton density fat fraction: a prospective study of 400 healthy volunteers. Radiology. 2020;294:89–97, http://dx.doi.org/10.1148/radiol.2019190467.
48. Doda Khera R, Homayounieh F, Lades F, Schmidt B, Sedlmair M, Primak A, et al. Can dual-energy computed tomography quantitative analysis and radiomics differentiate normal liver from hepatic steatosis and cirrhosis? J Comput Assist Tomogr. 2020;44:223–9, http://dx.doi.org/10.1097/rct.0000000000000989.
49. Bottari A, Silipigni S, Carerj ML, Cattafi A, Maimone S, Marino MA, et al. Dual-source dual-energy CT in the evaluation of hepatic fractional extracellular space in cirrhosis. Radiol Med. 2020;125:7–14, http://dx.doi.org/10.1007/s11547-019-01089-7.
50. Aggarwal A, Singbal SB, Yiew DSS, Quek ST, Wang S, Junwei Z. Pigmented villonodular synovitis: novel role of dual-energy CT. Clin Rheumatol. 2020;26:e113–4, http://dx.doi.org/10.1097/RHU.0000000000000980.
51. Kosmala A, Weng AM, Krauss B, Knop S, Bley TA, Petritsch B. Dual-energy CT of the bone marrow in multiple myeloma: diagnostic accuracy for quantitative differentiation of infiltration patterns. Eur Radiol. 2018;12:5083–90, http://dx.doi.org/10.1007/s00330-018-5537-5.
52. Kosmala A, Weng AM, Heidemeier A, Krauss B, Knop S, Bley TA, et al. Multiple myeloma and dual-energy CT: diagnostic accuracy of virtual noncalcium technique for detection of bone marrow infiltration of the spine and pelvis. Radiology. 2018;1:205–13, http://dx.doi.org/10.1148/radiol.2017170281.
53. Huang HC, Srinivasan R, Sun Y, Kazakia GJ, Lin PC, Yeh BM. Detection of lumbar spine osseous metastases using dual-energy CT: Phantom results and preliminary clinical validation. AJR Am J Roentgenol. 2019;212:402–10, http://dx.doi.org/10.2214/ajr.18.19933.
54. Kim SM, Chang SA, Shin W, Choe YH. Dual-energy CT perfusion during pharmacologic stress for the assessment of myocardial perfusion defects using a second-generation dual-source CT: a comparison with cardiac magnetic resonance imaging. J Comput Assist Tomogr. 2014;38:44–52, http://dx.doi.org/10.1097/rct.0b013e3182a77626.
55. Abadia AF, van Assen M, Martin SS, Vingiani V, Griffith LP, Giovagnoli DA, et al. Investigation of myocardial extracellular volume fraction in heart failure patients using iodine map with rapid-kV switching dual-energy CT: segmental comparison with MRI T1 mapping. J Cardiovasc Comput Tomogr. 2019;24:S1934–5925, http://dx.doi.org/10.1016/j.jcct.2019.12.032.
56. Kumar V, Harfi TT, He X, McCarthy B, Cardona A, Simonetti OP, et al. Estimation of myocardial fibrosis in humans with dual energy CT. J Cardiovasc Comput Tomogr. 2019;6:315–8, http://dx.doi.org/10.1016/j.jcct.2018.12.004.
57. Lee HJ, Im DJ, Youn JC, Chang S, Shu YJ, Hong YJ, et al. Myocardial extracellular volume fraction with dual-energy equilibrium contrast-enhanced cardiac CT in nonischemic cardiomyopathy: a prospective comparison with cardiac MR imaging. Radiology. 2016;1:49–57, http://dx.doi.org/10.1148/radiol.2016151289.
58. Jacobsen MC, Cressman ENK, Tamm E, Baluya DL, Duan X, Cody DD, et al. Dual-energy CT: lower limits of iodine detection and quantification. Radiology. 2019;2:414–9, http://dx.doi.org/10.1148/radiol.2019182870.
59. Johnson TR, Himsl I, Hellerhoff K, Mayr D, Rjosk-Dendorfer D, Ditsch N, et al. Dual-energy CT for the evaluation of silicone breast implants. Eur Radiol. 2013;23:991–6, http://dx.doi.org/10.1007/s00330-012-2667-z.
60. Glazebrook KN, Doerge S, Leng S, Drees TA, Hunt KN, Zingula SN, et al. Ability of dual-energy CT to detect silicone gel breast implant rupture and nodal silicone spread. AJR Am J Roentgenol. 2019;212:933–42, http://dx.doi.org/10.2214/ajr.18.20138.